THE JOURNAL OF PHYSICAL CHEMISTRY Letters

Letter

pubs.acs.org/JPCL

Stark Ionization of Atoms and Molecules within Density Functional Resonance Theory

Ask Hjorth Larsen,*[,†] Umberto De Giovannini,*[,†] Daniel L. Whitenack,[‡] Adam Wasserman,*[,¶,‡] and Angel Rubio*[,†]

[†]Nano-Bio Spectroscopy Group and ETSF Scientific Development Centre, Departamento de Física de Materiales, Universidad del País Vasco, CSIC-UPV/EHU-MPC and DIPC, Avenida de Tolosa 72, E-20018 San Sebastián, Spain

[‡]Department of Physics, Purdue University, 525 Northwestern Avenue, West Lafayette, Indiana 47907, United States

[¶]Department of Chemistry, Purdue University, 560 Oval Drive, West Lafayette, Indiana 47907, United States

ABSTRACT: We show that the energetics and lifetimes of resonances of finite systems under an external electric field can be captured by Kohn–Sham density functional theory (DFT) within the formalism of uniform complex scaling. Properties of resonances are calculated self-consistently in terms of complex densities, potentials, and wave functions using adapted versions of the known algorithms from DFT. We illustrate this new formalism by calculating ionization rates using the complex-scaled local density approximation and exact exchange. We consider a variety of atoms (H, He, Li, and Be) as well as the H_2 molecule. Extensions are briefly discussed.

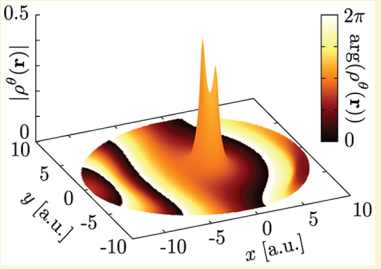

SECTION: Spectroscopy, Photochemistry, and Excited States

The description of metastable compounds has been elusive to first-principles calculations due to the lack of a variational principle. The concepts of metastability and long-lived resonances (or tunneling processes) are closely related, and in the end, we are facing the description of the lifetime of a given open quantum system. One approach to such calculations is the complex-scaling method, pioneered by Aguilar, Balslev, and Combes.[1,2] Within this formalism, resonances appear as the result of a complex scaling $\mathbf{r} \rightarrow \mathbf{r}e^{i\theta}$ of the real-space coordinates in the Hamiltonian. The method has been used to calculate resonance energies and lifetimes of negative ions of atoms,[3] as well as resonances induced by static electric fields.[4,5]

Applications have however generally been limited to small systems or systems with reduced dimensionality due to the computational difficulty of solving many-particle problems. A different approach must be taken to accommodate realistic systems with many electrons. Recently, it has been proven that the low-lying metastable states of a given system can be described within a density functional framework once we allow for complex densities.[6] An analogue of the Hohenberg–Kohn theorem then allows for the calculation of the lowest-energy resonance of a system. On the basis of this, the first Kohn–Sham (KS) density functional resonance theory (DFRT) calculations have since been published, although limited to 1D systems with one or two electrons.[7,8]

A notable ongoing development, termed complex DFT (CODFT), is based on complex absorbing potentials.[9,10] This method relies on the definition of an absorption zone outside of the system boundary to calculate lifetimes based on how wave functions extend into the absorbing region. Another method is exterior complex scaling, where a complex coordinate scaling is applied outside of a certain radius.[11]

The method presented in this Letter is based on uniform complex scaling, where all regions of space are treated equally. We present first-principles DFRT calculations of Stark resonance states and lifetimes in real 3D systems within exact exchange (EXX) and the local density approximation (LDA). We consider the H, He, Li, and Be atoms and the H_2 molecule within strong electric fields, extending the method beyond the model systems for which it has been demonstrated previously.[7,8] The implementation is open source and part of the DFT code Octopus.[12,13] Wave functions are represented on real-space grids, and atoms are represented by pseudopotentials. Atomic units are used throughout this Letter.

We describe first how complex scaling is incorporated within DFT and then present the major algorithmic steps involved. Finally, we discuss the results.

The complex-scaling transformation $\mathbf{r} \rightarrow \mathbf{r}e^{i\theta}$ changes the Hamiltonian of a system into a non-Hermitian operator $\hat{H}^\theta$, affecting bound and unbound eigenstates differently. The energy of any bound state is conserved, while that of a non-normalizable, unbound state changes. As θ is increased from 0, resonances can be uncovered from among the continuum as localized eigenstates of $\hat{H}^\theta$. From the corresponding complex eigenvalues $\epsilon = \epsilon_{res} - i\Gamma/2$, the ionization rate is given by Γ; see, for example, the review by Reinhardt.[14]

Received: May 29, 2013
Accepted: July 31, 2013
Published: July 31, 2013

   dx.doi.org/10.1021/jz401110h | J. Phys. Chem. Lett. 2013, 4, 2734–2738

Standard KS DFT is formulated as the minimization of an energy functional over a set of auxiliary single-particle states. Correspondingly, we take the complex-valued KS energy functional[8] to be

$$E_{\mathrm{res}} - \mathrm{i}\frac{\Gamma}{2} = \mathrm{e}^{-\mathrm{i}2\theta}\sum_n \int \psi_n^\theta(\mathbf{r})\left(-\frac{1}{2}\nabla^2\right)\psi_n^\theta(\mathbf{r})\,\mathrm{d}\mathbf{r} + \mathrm{e}^{-\mathrm{i}\theta}\frac{1}{2}\iint \frac{n^\theta(\mathbf{r})n^\theta(\mathbf{r}')}{\|\mathbf{r}-\mathbf{r}'\|}\,\mathrm{d}\mathbf{r}\,\mathrm{d}\mathbf{r}' + E_{\mathrm{xc}}^\theta[n^\theta] + \int v_{\mathrm{ext}}^\theta(\mathbf{r})n^\theta(\mathbf{r})\,\mathrm{d}\mathbf{r} \tag{1}$$

where E_{res} is the resonance energy and Γ the ionization rate inverse lifetime. Γ represents a total over all metastable single-electron states in the system. Above, we have introduced complex-scaled KS states $\psi_n^\theta(\mathbf{r})$, the density $n^\theta(\mathbf{r})$, and operators $\hat{O}^\theta(\mathbf{r})$ (such as $v_{\mathrm{ext}}^\theta(\mathbf{r})$ and the kinetic operator), which are analytic continuations

$$\psi^\theta(\mathbf{r}) = \mathrm{e}^{\mathrm{i}3\theta/2}\psi(\mathbf{r}\mathrm{e}^{\mathrm{i}\theta}) \tag{2}$$

$$n^\theta(\mathbf{r}) = \sum_n [\psi_n^\theta(\mathbf{r})]^2 = \mathrm{e}^{\mathrm{i}3\theta}n(\mathbf{r}\mathrm{e}^{\mathrm{i}\theta}) \tag{3}$$

$$\hat{O}^\theta(\mathbf{r}) = \hat{O}(\mathbf{r}\mathrm{e}^{\mathrm{i}\theta}) \tag{4}$$

of their unscaled equivalents. We have used that bra states are not conjugated[15] and that left and right eigenstates are equal because the complex-scaled Hamiltonian of a finite system is complex-symmetric. This is always the case when the initial, unscaled Hamiltonian contains only real terms. These definitions ensure that integrals such as matrix elements are unaffected by the scaling angle θ under appropriate conditions.[14] Thus, eq 1 reduces to the ordinary KS energy functional if the system is bound.

For unbound systems, the energy functional is complex and therefore does not possess a minimum. However, the lowest resonance can still be obtained by requiring the functional to be stationary.[6] Taking the derivative with respect to the wave functions $\psi_n^\theta(\mathbf{r})$ yields a set of KS equations

$$\hat{H}^\theta\psi_n^\theta(\mathbf{r}) = \left[-\frac{1}{2}\mathrm{e}^{-\mathrm{i}2\theta}\nabla^2 + v^\theta(\mathbf{r})\right]\psi_n^\theta(\mathbf{r}) = \epsilon_n\psi_n^\theta(\mathbf{r}) \tag{5}$$

where the effective potential $v^\theta(\mathbf{r})$ is the sum of the complex-scaled Hartree, XC, and external potentials,[8] $v^\theta(\mathbf{r}) = v_{\mathrm{H}}^\theta(\mathbf{r}) + v_{\mathrm{xc}}^\theta(\mathbf{r}) + v_{\mathrm{ext}}^\theta(\mathbf{r})$. A self-consistency loop is then formulated from these quantities. For each calculation, a fixed value of θ is chosen. θ should be large enough for the resonant states to emerge but can otherwise be chosen to optimize the numerics.[16,17] In the DFRT calculations presented here, θ is chosen by testing different values with different grid spacings to find a combination with good numerical precision. This is similar to the convergence checks performed in standard DFT, but more important, because the numerical error must be made smaller than the imaginary part of the energy, which can be quite close to zero. For this reason, a fine grid is required to calculate low ionization rates.

XC functionals $E_{\mathrm{xc}}^\theta[n^\theta]$ can be derived by analytic continuation consistently with eqs 2−4. Consider, for example, spin-paired LDA. The XC energy is complex-scaled by rotating the integration contour from the real axis into the complex plane,

$$E_{\mathrm{xc}}[n] = \int n(\mathbf{r})\epsilon(n(\mathbf{r}))\,\mathrm{d}\mathbf{r} = \int n(\mathbf{r}\mathrm{e}^{\mathrm{i}\theta})\epsilon(n(\mathbf{r}\mathrm{e}^{\mathrm{i}\theta}))\,\mathrm{d}\mathbf{r}\,\mathrm{e}^{\mathrm{i}3\theta} \tag{6}$$

which is also a functional E_{xc}^θ of $n^\theta(\mathbf{r})$ by eq 3. The potential follows as $v_{\mathrm{xc}}^\theta(\mathbf{r}) = \delta E_{\mathrm{xc}}^\theta[n^\theta]/\delta n^\theta(\mathbf{r})$. Thus, the exchange part of the potential becomes

$$v_{\mathrm{x}}^\theta(\mathbf{r}) = -\left(\frac{3}{\pi}\right)^{1/3}\mathrm{e}^{-\mathrm{i}\theta}[n^\theta(\mathbf{r})]^{1/3} = v_{\mathrm{x}}(\mathbf{r}\mathrm{e}^{\mathrm{i}\theta}) \tag{7}$$

as in eq 4. Due to the complex cube root, the exchange potential is three-valued. However, the potential is the complex continuation of a corresponding real potential for $\theta = 0$ and therefore must remain continuous. Further, because the complex scaling operation leaves the origin $\mathbf{r} = 0$ unaffected, $v_{\mathrm{x}}^\theta(0)$ must be real and independent of θ. Starting at $\mathbf{r} = 0$, we therefore evaluate $v_{\mathrm{x}}^\theta(\mathbf{r})$ as the principal branch of the cube root of the density. For some $\mathbf{r}$, the density may approach a branch point; therefore, the function becomes discontinuous. This situation is illustrated in Figure 1, where the three branches,

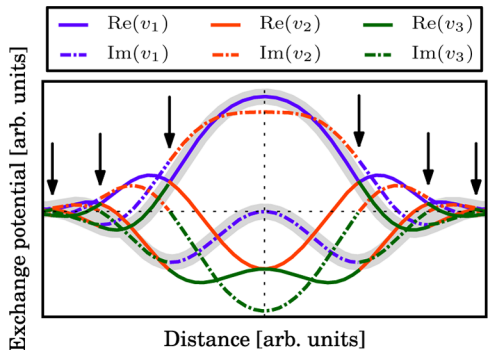

Figure 1. Real and imaginary parts of the three branches v_1, v_2, and v_3 of the LDA exchange potential generated by a complex-scaled Gaussian density. The branches are stitched together to form one continuous exchange potential, indicated by the shaded bands. Arrows indicate the branch points.

evaluated from a Gaussian density with $\theta = 0.5$, have different colors. At a branch point, one can always choose another branch such that the resulting, *stitched* potential becomes continuous and yields the correct energy $E_{\mathrm{x}}^\theta[n^\theta]$, which does not depend on θ.

Consider next the Perdew−Wang parametrization of correlation.[18] The correlation potential is expressed in terms of the Wigner−Seitz radius $[r_{\mathrm{s}}(\mathbf{r})]^{1/2} \sim [n(\mathbf{r})]^{-1/6}$ and takes the form

$$v_{\mathrm{c}}(r_{\mathrm{s}}) = \epsilon_{\mathrm{c}}(r_{\mathrm{s}}) - \frac{1}{3}\frac{\mathrm{d}\epsilon_{\mathrm{c}}(r_{\mathrm{s}})}{\mathrm{d}r_{\mathrm{s}}}r_{\mathrm{s}} \tag{8}$$

where

$$\epsilon_{\mathrm{c}}(r_{\mathrm{s}}) = -2A(1+\alpha_1 r_{\mathrm{s}})\ln\left(1+\frac{1}{Q_1(r_{\mathrm{s}})}\right) \tag{9}$$

$$Q_1(r_{\mathrm{s}}) = 2A\sum_{i=1}^{4}\beta_i r_{\mathrm{s}}^{i/2} \tag{10}$$

Here A, α_1, and β_{1-4} are real constants. This expression is straightforward to complex-scale using the stitching method already presented. We first evaluate $(r_{\mathrm{s}})^{1/2}$ at each point on the

dx.doi.org/10.1021/jz401110h | J. Phys. Chem. Lett. 2013, 4, 2734−2738

real-space grid by stitching $[n^{\theta}(\mathbf{r})]^{-1/6}$. Then, the complex logarithm $\ln(1 + 1/Q_1(r_s))$ is stitched to obtain $\epsilon_c(r_s)$. Other local or semilocal (GGA) functionals can be similarly complex-scaled.

One of the challenges in KS DFRT is to reliably determine which states should be occupied, as the complex eigenvalues have no natural ordering. Consider independent particles in 1D near an atom represented by a soft Coulomb potential with charge Z in a uniform electric field of strength F. This system has the external potential $Fxe^{i\theta} - Z/(x^2e^{i2\theta} + \alpha^2)^{1/2}$. Figure 2

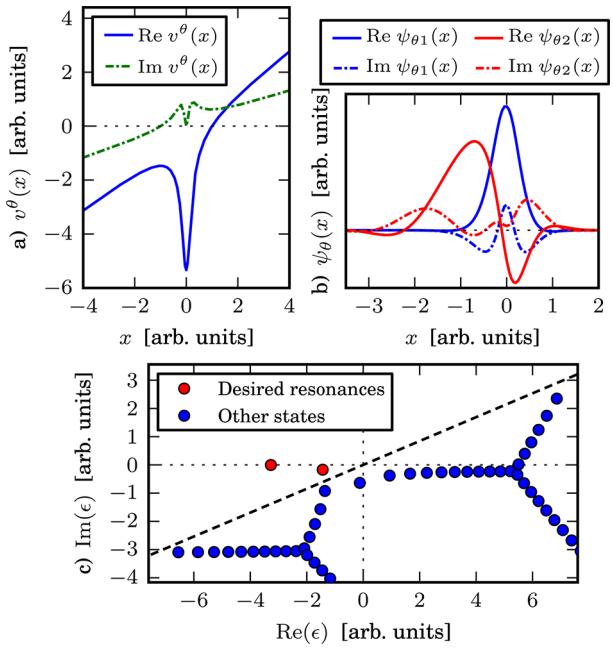

Figure 2. (a) Real and imaginary parts of the complex-scaled potential. (b) Real and imaginary parts of the lowest resonance wave functions. (c) The spectrum. The dashed line arg $Z = \theta$ separates the two real resonances (red) with imaginary parts of -2.6×10^{-3} and -0.17 from the remaining eigenstates (blue), which are artifacts of the simulation box or continuum.

shows (a) the complex-scaled potential, (b) wave functions, and (c) eigenvalues for $F = 4$, $Z = 4$, $\alpha = 0.15$, and $\theta = 0.4$ in a simulation box of size 10. In the spectrum in Figure 2c, the dashed line arg $Z = \theta$ divides the complex plane in two parts. On the upper left side, there are two eigenvalues that correspond to physical resonances. These states would have been bound if no electric field had been applied to the system but are now situated just below the real axis. Below the dashed line arg $Z = \theta$, the spectrum forms a system of lines. It has been demonstrated by Cerjan and co-workers[16,19] that the numerical range (the set of values $(\psi^{\theta}|H^{\theta}_{\text{stark}}|\psi^{\theta})$ for all normalized states ψ^{θ}) of the complex-scaled Stark Hamiltonian, and thus its entire continuous spectrum, falls within this region. The discrete eigenvalues above the line arg $Z = \theta$ can therefore be identified as originating from bound states in the isolated atom and can now be assigned occupations in order of the increasing real (or negative imaginary) part of the energy while the remaining states are left unoccupied. In practical calculations using iterative eigensolvers, particularly when far away from self-consistency, eigenvalues originating from the continuum may appear above the line arg $Z = \theta$. As these states should not be occupied, we use a simple rule to identify them. They are occupied in ascending order of Re $\epsilon + \alpha(\text{Im } \epsilon)^2$, where α is a tunable parameter. The value $\alpha = 2/\sin\theta$ generally works for the atoms considered here.

Like in standard DFT calculations, it is the outermost (valence) electrons that determine most properties of a system. Nuclear point charges cause numerical difficulties due to their central singularity. Pseudopotentials solve this problem by replacing the point charges by smooth charge distributions, while making sure to account properly for the core−valence interaction. Here, we use the normconserving Hartwigsen−Goedecker−Hutter (HGH) pseudopotentials.[24] They can be explicitly complex-scaled because they are parametrized as polynomials and Gaussians. In the calculations below, we use the potentials that include all electrons as valence electrons while only smoothening the nuclear potential (Li and Be have three and four valence electrons, respectively). With this choice, the approach is demonstrated on systems with more than one occupied KS state. The approach is also compatible with standard frozen-core pseudopotentials.

Figure 3a shows the ionization rate for He as a function of electric field strength calculated using various methods. The

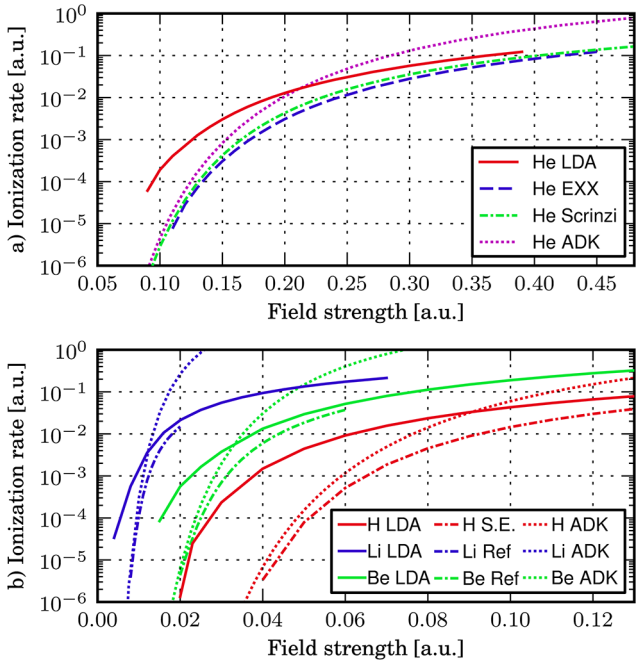

Figure 3. Ionization rates (1 a.u. $\approx 4.13 \times 10^{16}$ s^{-1}) of (a) He and (b) H, Li, and Be as a function of electric field strength (1 a.u. $\approx 5.14 \times 10^{11}$ V/m). Rates are calculated using DFRT (LDA or EXX) and the Ammosov−Delone−Krainov (ADK) method.[20] Rates of H are also calculated by solving the complex-scaled Schrödinger equation. Accurate reference rates from first-principles methods are shown for He,[21] Li,[22] and Be.[23].

reference results are based on direct solution of the complex-scaled two-particle Schrödinger equation and thus represent the closest to an exact calculation.[21] The DFRT rates Γ for LDA and EXX are obtained directly from eq 1 after solving eq 5 self-consistently for the complex density using $\theta = 0.35$. A value of θ is suitable if it is large enough to localize the resonant KS states and if the results converge rapidly with grid spacing. A very fine grid spacing of 0.08 a.u. is still needed to converge the lowest rates. The LDA substantially overestimates the ionization rate, particularly for small fields, while EXX is in very good agreement with the reference. EXX results are obtained by

dx.doi.org/10.1021/jz401110h | J. Phys. Chem. Lett. 2013, 4, 2734−2738

setting the exchange energy to minus half of the Hartree energy, which is exact for two-electron systems.

Also shown are results from the Ammosov−Delone−Krainov (ADK) method.[20] This is a simple approximation for ionization rates in atoms, based on the atomic ionization potential. ADK is accurate for low fields because the ionization rate is strongly linked to the ionization potential in this limit. However, it greatly overestimates rates for large fields. We attribute the inaccuracy of LDA for low fields to its well-known underestimation of ionization potentials, taken as minus the energy of the highest occupied KS orbital (0.57 hartree from LDA versus 0.92 from EXX and 0.90 from experiment). This error of LDA is ultimately linked to the exponential rather than Coulomb-like decay of the potential.[25] Note that more accurate ionization potentials can be calculated by subtracting the total energy of the charged and the neutral system. Ionization rates based on this method have been presented with CODFT.[9]

Similarly calculated ionization rates with LDA and ADK are shown for H, Li, and Be in Figure 3b along with reference values for H from ordinary one-particle calculations and for Li[22] and Be.[23] Generally, the atoms with lower atomization potentials have higher ionization rates, and again, a large discrepancy shows between ADK and LDA for low fields.

Figure 4 shows ionization rates for the H_2 molecule as a function of internuclear distance calculated for different field strengths with LDA and EXX. The molecular axis is parallel to the electric field. The nuclei are described as fixed point particles; therefore, only the static electron ionization yield is calculated. The reference calculations by Saenz[26] correspond to an accurate solution of the two-particle complex-scaled Schrödinger equation.

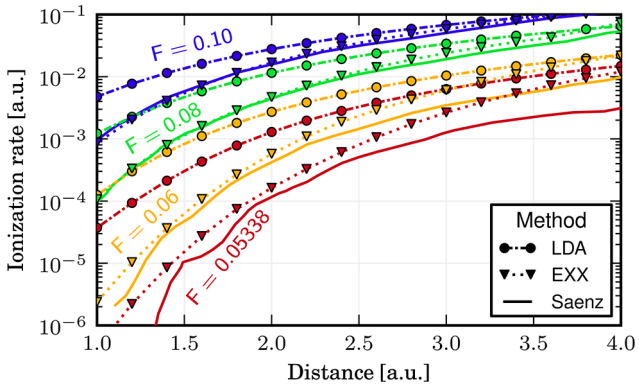

Figure 4. Ionization rate of H_2 as a function of internuclear distance. Different methods are denoted by different line and point styles, while colors denote different static field strengths in atomic units.

H_2 in the dissociation limit is a pathological case in DFT as the system is dominated by strong static correlations that most functionals fail to capture. In this limit, the system consists of two isolated, charge-neutral atoms. A static calculation with an electric field will produce a different solution where both electrons reside on the atom favored by the field, although the situation at intermediate distances as here is more complicated.

LDA again overestimates ionization rates, particularly for short bond lengths. For large field strength and short bond lengths, the agreement between EXX and the reference is almost perfect. However, ionization rates on the order of 10^{-5} au lose accuracy due to the numerical dependence of energy on θ. This error can be eliminated by optimizing the choice of θ and using a finer grid spacing[16] (0.1 Bohr with $\theta = 0.22$ for the data points in question). We attribute most of the disagreement at short bond lengths between EXX and the reference to this error.

At large bond lengths and large field strength, the EXX agrees well with the reference. This corresponds to the case where both electrons reside mostly on the same atom. For smaller field strengths, the system corresponds more closely to the strongly correlated case, and the error is larger.

The accuracy of the XC approximation is clearly a determining factor for the quantitative success of DFRT. We have here considered very simple functionals, and, in particular, LDA exhibits large errors. Phenomena of excited states depend intricately on the decay properties of the potential far from the system, which are difficult to describe with semilocal functionals. A promising method to solve this problem is to introduce a fictitious "XC density", which defines a correction to the XC potential, giving it a Coulomb-like decay.[27] This can greatly improve the accuracy of ionization rates. We expect the derivation of improved XC functionals for DFRT to be one of the next major steps in the development of this method.

The presented calculations demonstrate the reliability and performance of DRFT for realistic atoms and dimers. The extension to other molecular systems and nanostructures is straightforward, opening the path toward a systematic study of the electronic and structural properties of metastable complexes. Furthermore, DFRT has implications for the discussion and analysis of resonances in molecular electronics as well as to the description of intermediates in surface−molecule interactions as the method introduces decay processes in a natural way into the widely used first-principles density functional framework.

A future goal is to enable DFRT calculations for time-dependent systems, where time propagation can be started from statically determined resonant states. This paves the road to tackle dynamical processes through metastable intermediates, as seen in the recently available ultrafast and ultraintense laser probes that allow one to extract temporal and spatial information of electron and ion dynamics[28] as well as imaging.[29,30]

AUTHOR INFORMATION

Corresponding Author

*E-mail: asklarsen@gmail.com (A.H.L.); umberto.degiovannini@ehu.es (U.D.G.); awasser@purdue.edu (A.W.); angel.rubio@ehu.es (A.R.).

Notes

The authors declare no competing financial interest.

ACKNOWLEDGMENTS

We acknowledge funding from The European Research Council Advanced Grant DYNamo (ERC-2010-AdG Proposal No. 267374), Grupo Consolidado UPV/EHU del Gobierno Vasco (IT578-13), the European Commission (Grant number 280879-2 CRONOS CP-FP7), and the Spanish Grants FIS2010-21282-C02-01 and PIB2010US-00652. D.L.W. and A.W. acknowledge funding from the U.S. National Science Foundation CAREER program Grant No. CHE-1149968.

REFERENCES

(1) Aguilar, J.; Combes, J. *Commun. Math. Phys.* **1971**, *22*, 269−279.
(2) Balslev, E.; Combes, J. *Commun. Math. Phys.* **1971**, *22*, 280−294.
(3) Moiseyev, N.; Corcoran, C. *Phys. Rev. A* **1979**, *20*, 814−817.

(4) Reinhardt, W. P. *Int. J. Quantum Chem.* **1976**, *10*, 359−367.
(5) Herbst, I. W.; Simon, B. *Phys. Rev. Lett.* **1978**, *41*, 67−69.
(6) Wasserman, A.; Moiseyev, N. *Phys. Rev. Lett.* **2007**, *98*, 093003.
(7) Whitenack, D. L.; Wasserman, A. *J. Phys. Chem. Lett.* **2010**, *1*, 407−411.
(8) Whitenack, D. L.; Wasserman, A. *Phys. Rev. Lett.* **2011**, *107*, 163002.
(9) Zhou, Y.; Ernzerhof, M. *J. Phys. Chem. Lett.* **2012**, *3*, 1916−1920.
(10) Zhou, Y.; Ernzerhof, M. *J. Chem. Phys.* **2012**, *136*, 094105.
(11) Simon, B. *Phys. Lett. A* **1979**, *71*, 211−214.
(12) Marques, M. A.; Castro, A.; Bertsch, G. F.; Rubio, A. *Comput. Phys. Commun.* **2003**, *151*, 60−78.
(13) Castro, A.; Appel, H.; Oliveira, M.; Rozzi, C. A.; Andrade, X.; Lorenzen, F.; Marques, M. A. L.; Gross, E. K. U.; Rubio, A. *Phys. Status Solidi B* **2006**, *243*, 2465−2488.
(14) Reinhardt, W. P. *Annu. Rev. Phys. Chem.* **1982**, *33*, 223−255.
(15) Moiseyev, N.; Certain, P.; Weinhold, F. *Mol. Phys.* **1978**, *36*, 1613−1630.
(16) Cerjan, C.; Hedges, R.; Holt, C.; Reinhardt, W. P.; Scheibner, K.; Wendoloski, J. J. *Int. J. Quantum Chem.* **1978**, *14*, 393−418.
(17) Whitenack, D. L.; Wasserman, A. *J. Chem. Phys.* **2012**, *136*, 164106.
(18) Perdew, J. P.; Wang, Y. *Phys. Rev. B* **1992**, *45*, 13244−13249.
(19) Cerjan, C.; Reinhardt, W. P.; Avron, J. E. *J. Phys. B: At. Mol. Phys.* **1978**, *11*, L201−L205.
(20) Ammosov, M. V.; Delone, N. B.; Krainov, V. P. *Zh. Eksp. Teor. Fiz.* **1986**, *91*, 2008−2013.
(21) Scrinzi, A.; Geissler, M.; Brabec, T. *Phys. Rev. Lett.* **1999**, *83*, 706−709.
(22) Nicolaides, C. A.; Themelis, S. I. *Phys. Rev. A* **1993**, *47*, 3122−3127.
(23) Themelis, S. I.; Nicolaides, C. A. *J. Phys. B: At., Mol. Opt. Phys.* **2000**, *33*, 5561−5580.
(24) Hartwigsen, C.; Goedecker, S.; Hutter, J. *Phys. Rev. B* **1998**, *58*, 3641−3662.
(25) van Leeuwen, R.; Baerends, E. J. *Phys. Rev. A* **1994**, *49*, 2421−2431.
(26) Saenz, A. *Phys. Rev. A* **2000**, *61*, 051402.
(27) Andrade, X.; Aspuru-Guzik, A. *Phys. Rev. Lett.* **2011**, *107*, 183002.
(28) Shafir, D.; Soifer, H.; Bruner, B. D.; Dagan, M.; Mairesse, Y.; Patchkovskii, S.; Ivanov, M. Y.; Smirnova, O.; Dudovich, N. *Nature* **2012**, *485*, 343−346.
(29) Zhou, X.; Ranitovic, P.; Hogle, C. W.; Eland, J. H. D.; Kapteyn, H. C.; Murnane, M. M. *Nat. Phys.* **2012**, *8*, 232−237.
(30) Hensley, C. J.; Yang, J.; Centurion, M. *Phys. Rev. Lett.* **2012**, *109*, 133202.